Published in final edited form as:
ACS Nano. 2010 February 23; 4(2): 1033–1041. doi:10.1021/nn901181c.

Exceptionally High Payload of Doxorubicin in Hollow Gold Nanospheres for Near-Infrared Light-Triggered Drug Release

Jian You[1,2], **Guodong Zhang**[1], and **Chun Li**[1,*]

[1]Department of Experimental Diagnostic Imaging, The University of Texas M. D. Anderson Cancer Center, Houston, Texas 77030

[2]On leave from College of Pharmaceutical Sciences, Zhejiang University, Yuhangtang Road 388, Hangzhou 310058, People's Republic of China

Abstract

We report dual-functional hollow gold nanospheres (HAuNS, ~40-nm diameter) capable of mediating both photothermal ablation of cancer cells and drug release upon near-infrared (NIR) light irradiation. As high as 63% DOX by weight (~1.7 μg DOX/μg Au) could be loaded to polyethylene glycol (PEG)-coated HAuNS since DOX was coated to both the outer and the inner surfaces of HAuNS. Irradiation with NIR laser induced photothermal conversion, which triggered rapid DOX release from DOX-loaded HAuNS. The release of DOX was also pH-dependent, with more DOX released in aqueous solution at lower pH. Significantly greater cell killing was observed when MDA-MB-231 cells incubated with DOX-loaded HAuNS were irradiated with NIR light, attributable to both HAuNS-mediated photothermal ablation and cytotoxicity of released free DOX.

Keywords

hollow gold nanospheres; doxorubicin; triggered release; near-infrared light; antitumor activity

Nanocarriers have been designed as a novel platform for the delivery of therapeutic agents. Among the drug carriers reported, liposomes and lipid nanospheres[1] have come onto the market. Polymeric drugs are currently in clinical trials.[2, 3] All of these are organic nanoparticles consisting of lipids and/or synthetic polymers. Whereas rapid progress has been made in the development of drug delivery systems using organic nanoparticles, relatively less progress has been made in the development of inorganic nanoparticle-based drug delivery systems. However, recent progress in the field of nanotechnology and nanofabrication has led to the identification of various inorganic nanoparticles as attractive vehicles for drug delivery, such as iron oxide nanoparticles for delivery of anticancer drugs (mitoxantrone[4] and doxorubicin[5]), carbon nanohorns for delivery of dexamethasone (an anti-inflammatory agent) [6] and cisplatin (an anticancer agent),[7] carbon nanotubes for delivery of anticancer drugs (paclitaxel,[8] platinum,[9, 10] and doxorubicin[11]), and gold nanoparticles. These inorganic nanoparticles have several advantages as drug carriers. First, they are easy to prepare with a defined size. More interestingly, they often exhibit multiple functions useful in medicine—for example, serving as exothermic reactors and contrast agents—whereas organic nanoparticles such as liposomes and polymer nanospheres serve only as drug reservoirs.

*Corresponding Author: Chun Li, Department of Experimental Diagnostic Imaging-Unit 59, The University of Texas M. D. Anderson Cancer Center, Houston, Texas 77030; Tel: 713-792-5182; Fax: 713-794-5456; cli@mdanderson.org.

Among the inorganic nanoparticles reported so far, gold nanoparticles (AuNP) have obtained the most attention for medicinal applications owing to their unique chemical and physical properties, including their functional versatility,[12] biocompatibility,[13] and low toxicity.[14, 15] AuNP are used for biosensing[16] and diagnostics.[17, 18] AuNPs also investigated as an attractive nanocarrier for delivery of various drugs into their targets. The payloads could be small drug molecules[19-21] or large biomolecules, such as proteins,[22, 23] DNA,[24] or RNA.[25, 26] Some groups have also reported the use of gold nanoparticles as drug carriers for doxorubicin (DOX) delivery and have shown enhanced cytotoxic effects with this approach *in vitro*.[27, 28]

Hollow gold nanospheres are a novel class of gold nanoparticles having plasmon absorption in the NIR region that display strong photothermal coupling property suitable for photothermal ablation(PTA) therapy. The unique combination of small size (30-50 nm in diameter), absence of a silica core, spherical shape, strong and tunable (520 - 950 nm) absorption band, and the lack of need for cytotoxic surfactant required to stabilize other gold nanoparticles suggest that HAuNS have the potential to be useful for *in vivo* molecular therapy. Indeed, we have recently demonstrated efficient active targeting of HAuNS and selective PTA of solid tumors in small animals using HAuNS directed at epidermal growth factor receptor (EGFR)[29] and melanocortin type-1 receptor overexpressed in melanoma.[30] These HAuNS exhibited excellent colloidal stability, enhanced tumor uptake, and efficient PTA effect against human tumor xenografts after intravenous injection.[29, 30]

However, although NIR light can penetrate several centimeters of tissues, its energy is gradually reduced as it travels deeper into tissues due to light scattering and absorption. Some tumor cells would inevitably receive sub-optimal laser exposure and may not be ablated. We hypothesized that the unique photothermal conversion property of HAuNS could be harnessed for modulating the delivery of anticancer drugs, thus making it possible to achieve significantly enhanced antitumor efficacy using two-punch approach in a single setting. In the work described herein, we investigated the utility of using HAuNS as a nanocarrier for DOX, and the potential application of DOX-loaded HAuNS (DOX@HAuNS) for anticancer therapy.

Results and Discussion

HAuNS were synthesized by sacrificial galvanic replacement of cobalt nanoparticles in the presence of chloroauric acid according to the method of Schwartzberg et al.[31] The average diameter of the resulting HAuNS was 38.5±1.7 nm, as determined by the dynamic light scattering method. Transmission electron microscopy (TEM) revealed the morphology of the HAuNS (Fig. 1A) and indicated that they had average diameter of 43±4.6 nm and average Au shell thickness of 4.0 nm. Surface modification by polyethylene glycol (PEG) resulted in a moderate increase in the average diameter of the HAuNS from 38.5±1.7 nm to 48.6±1.3 nm. Compared with HAuNS, PEG-HAuNS had a significantly increased colloidal stability: no aggregation was observed when PEG-HAuNS were stored in water at room temperature over a period of 3 months. The absorption spectra showed that the plasma resonance peaks for both HAuNS and PEG-HAuNS were tuned to the NIR region (~800 nm) (Fig. 1B). Thus, PEG modification did not affect the spectrum characteristic of HAuNS but did increase their physical stability.

The complexes of DOX@HAuNS and DOX@PEG-HAuNS were readily formed by simple mixing of HAuNS or PEG-HAuNS solutions with DOX for 24 h at room temperature and then repeated washing to remove unbound DOX. TEM images clearly showed a DOX layer with a thickness of about 4-6 nm covering the surface of both DOX@HAuNS and DOX@PEG-HAuNS, which did not exist in HAuNS and PEG-HAuNS prior to DOX coating (Fig. 1A). The color of the HAuNS changed from greenish to henna upon absorption of DOX. DOX@HAuNS displayed a UV–Vis absorption peak at 490 nm characteristic of DOX and a

broad NIR plasmon absorption peak at ~800 nm characteristic of HAuNS (Fig. 1C). At 24 h after mixing, the absorbance peak intensity of DOX in the UV-visible region was significantly reduced compared with the absorbance peak intensity immediately after mixing of DOX and HAuNS (0 h), when DOX was unbound (Fig. 1D). In addition, compared to free DOX, which exhibited strong fluorescence emission, the fluorescence signal from DOX in DOX@HAuNS was almost completely quenched (Fig. 1D, inset), a phenomenon known to occur when fluorophores are attached to a metal nanoparticle surface with close proximity.[32] These results indicate that DOX was tightly bound to HAuNS and PEG-HAuNS after 24 h incubation.

Figure 2A shows Langmuir adsorption isotherms at room temperature for the adsorption of DOX by HAuNS and PEG-HAuNS. PEG modification on HAuNS significantly affected DOX's absorbing efficiency. At a lower PEG coating density (PEG:Au molar ratio = 0.008:1), PEGylation of HAuNS resulted in higher DOX loading. However, the loading efficiency of DOX decreased with increasing PEG coating density. This may be explained by increased surface area as a result of increased colloidal stability and thus reduced population of aggregates formed among HAuNS when a small amount of PEG was introduced to the HAuNS surface. With excessive PEG modification, however, interaction between HAuNS and DOX was impeded because the steric hindrance of PEG prevented DOX molecules from approaching the surface of HAuNS. The saturation of DOX absorption to PEG-HAuNS at higher PEG coating densities (PEG:Au molar ratio = 0.04:1 and 0.125:1) suggests that the surface of HAuNS was completely occupied by DOX and PEG molecules under such conditions, whereas at the lower PEG coating density (PEG:Au molar ratio = 0.008:1), the DOX absorption isotherm did not plateau up to an initial DOX amount of 180 μg. Further increase in DOX payload is possible for this particular formulation. At the DOX amount of 180 μg in the initial DOX-HAuNS mixtures, the drug contents absorbed to HAuNS were 41%, 63%, and 27% for HAuNS, PEG-HAuNS (PEG:Au molar ratio = 0.008:1), and PEG-HAuNS (PEG:Au molar ratio = 0.125:1), respectively, corresponding to weight ratios of 0.69, 1.7, and 0.37 between DOX and gold (Fig. 2B). DOX loading to HAuNS and PEG-HAuNS led to an increase in the size of the nanoparticles, suggesting that the presence of DOX reduced the colloidal stability of these nanoparticles. DOX@HAuNS having higher PEG density were more stable than DOX@HAuNS having lower PEG density, which in turn were more stable than HAuNS without PEG coating (Fig. 2B). In the following descriptions of our studies, “PEG-HAuNS” refers to PEG-HAuNS with PEG:Au molar ratio of 0.008:1 unless specified otherwise.

In addition to colloidal stability, we also examined the stability of absorbed DOX on HAuNS and PEG-HAuNS. After an initial release of 15%-20% over the first 2-day period, no further release of DOX from either DOX@HAuNS or DOX@PEG-HAuNS was observed in water, phosphate-buffered saline (PBS, pH 7.0), or cell culture medium containing 10% fetal bovine serum over the second 2-day period (Fig. 2C). These results indicated that DOX was stably absorbed to HAuNS and PEG-HAuNS.

To investigate the mechanism of DOX binding to HAuNS, the amino group in DOX was blocked by an acetyl protecting group. The binding of DOX-acetamide to HAuNS was reduced to nearly zero (Fig. 2D), suggesting that the amino group of DOX was key for its high payload onto HAuNS. According to synthesis protocol, HAuNS were stabilized by negatively charged citrate with a zeta potential of -25 mA in PBS solution (pH 7.4). On the other hand, DOX was positively charged at pH 7.4. As a result, DOX was absorbed onto HAuNS via electrostatic interaction. The formation of complexes between drug molecules and nanocarriers is advantageous compared to covalent conjugation approach owing to easy fabrication and scale up, low cost, and predictable release profile.[19, 33]

DOX release from DOX@HAuNS and DOX@PEG-HAuNS could be readily controlled by using NIR laser. After the first NIR laser irradiation (begun at 1 h) at 4.0 W/cm^2 output power

for 5 min, the cumulative release, defined as the ratio of released DOX to total loaded DOX expressed as a percentage, increased from 4.1% to 22.2% for DOX@HAuNS and from 4.1% to 31.9% DOX for DOX@PEG-HAuNS (Fig. 3A). Release of DOX was significantly reduced or almost completely stopped when the NIR laser was switched off over the next 1 h of incubation. Similar results were observed when the laser treatment protocol was repeated beginning at 2 h. However, there was less DOX released during the second treatment cycle. By the third treatment cycle (beginning at 3 h), almost no DOX was released. These data suggested that DOX release from both DOX@HAuNS and DOX@PEG-HAuNS could be triggered by external NIR laser.

After NIR laser irradiation of DOX@HAuNS (~1.0×10^{12} particles/mL), the peak absorption intensity at around 490 nm was significantly increased, indicating release of free DOX from the nanocomplexes. The color of DOX@HAuNS changed from brown to green due to detachment of DOX from DOX@HAuNS (Fig. 3B). After centrifugal removal of free DOX, the remaining HAuNS solution displayed an absorption spectrum similar to that of DOX@HAuNS acquired prior to NIR laser irradiation but at a lower intensity, and with loss of the characteristic peak absorption of DOX at 490 nm (Fig. 3B). The reduced peak intensity at 800 nm after NIR laser irradiation may be attributed to fragmentation of a small fraction of HAuNS particles (data not shown).

Because DOX was attached to HAuNS via electrostatic interaction, it was anticipated that the release of DOX from DOX@HAuNS and DOX@PEG-HAuNS would be pH-dependent. Indeed, while there was no DOX released from DOX@PEG-HAuNS in PBS at pH 10 and only 11% DOX released in PBS at pH 7.4 at room temperature after 2 days of incubation, the DOX release reached 35% at pH 5.0 and 57% at pH 3.0 (Fig. 3C). The observed pH dependency is attributed to the increased hydrophilicity and higher solubility of DOX at lower pH caused by increased protonation of -NH_2 groups on DOX, which reduce the interaction between DOX and HAuNS. When the pH was decreased, the COO^- groups on the surface of HAuNS also became protonated. As a result, the electrostatic interaction between DOX and HAuNS was reduced. The pH-dependent drug release from HAuNS or PEG-HAuNS could be exploited for drug delivery applications: the microenvironments of extracellular tissues of tumors and intracellular lysosomes and endosomes are acidic, and this acidity could facilitate active drug release from HAuNS-based delivery vehicles.

NIR laser irradiation increased the amount of DOX released from DOX@HAuNS or DOX@PEG-HAuNS incubated in PBS at different pH levels; the lower the pH of the medium, the less DOX released. For example, after 5 min of continuous NIR laser irradiation at 4.0 W/cm^2, 14.6%, 16.7%, and 5.1% more DOX was released from DOX@HAuNS when the nanoparticles were incubated in PBS at pH 7.4, pH 5.0, and pH 3.0, respectively (Fig. 3D). The ability to achieve higher DOX release with NIR light at pH ~5.0 is favorable because the intracellular lysosome environment of tumor cells has a pH of approximately 5.0.[34]

To explain the observed high loading capacity of DOX to HAuNS and further evaluate the advantages of HAuNS as drug carriers, we compared the DOX loading efficiency and drug release behavior between HAuNS and AuNPs having similar size (~40 nm) and surface charge (zeta potential ~ -25 mA). HAuNS or AuNPs with the same equivalent Au concentration were incubated with DOX (final concentration of 1.0 mM). On the basis of 1.0 μg Au, the DOX payload increased from ~0.2 μg in AuNPs to 0.7 μg in HAuNS, a 3.5-fold increase (Fig. 4A). This increase can be explained by the greater surface area of HAuNS compared to AuNPs. Assuming that the shell thickness of HAuNS is 4.0 nm and the diameter of both HAuNS and AuNP is 40 nm, it is estimated that each solid AuNP is equivalent to two hollow HAuNS on the basis of weight. This means that HAuNS should have twice the DOX payload of AuNPs if all DOX molecules are coated on the outer surface of HAuNS. The fact that 3.5-fold higher

DOX was found bound to HAuNS suggests that the inner surface of HAuNS was also coated with DOX. In fact, it is estimated that HAuNS possess 3.2-fold greater surface area than AuNPs when the inner and outer surface areas are counted. TEM showed that the shell of HAuNS was porous (Fig. 1A), which makes it possible for DOX molecules to diffuse into the core and bind to the inner surface of HAuNS.

In addition to significant difference in DOX loading capacity between HAuNS and AuNP, DOX@HAuNS also displayed distinct characteristic of NIR light-triggered DOX release. In contrast, no DOX release was observed when DOX-coated AuNP was irradiated with NIR light (Fig. 4B). This is because unlike DOX@HAuNS, there was no plasmon absorption in the NIR region for DOX@AuNP (Fig. 4C). When aqueous solutions of HAuNS, DOX@HAuNS, and DOX@PEG-HAuNS having the same nanoparticle concentration of 0.7×10^{11} particles/mL were exposed to NIR light (5.0 W/cm^2 for 10 min), the temperature was increased 39°C, 27°C, and 30°C, respectively. In comparison, no significant temperature change was observed when PBS or solution of AuNP was exposed to the NIR laser (Fig. 4D). Thus, the temperature elevation mediated by HAuNS in the presence of NIR light may be responsible for NIR laser–triggered release of DOX from DOX@HAuNS and DOX@PEG-HAuNS.

Both DOX@HAuNS and DOX@PEG-HAuNS were internalized into MDA-MB-231 cells and were retained in the endolysosomal compartments. After 1 h incubation, DOX@HAuNS showed strong red fluorescence signal from DOX despite quenching effect with DOX bound to HAuNS. The fluorescence signal was limited to spots scattered throughout the cytoplasm. The white bright dots obtained from dark-field imaging indicated the presence of HAuNS, which to a large extent colocalized with DOX (Fig. 5A). These results suggested that HAuNS together with DOX were phagocytosed by the cancer cells and distributed to the endolysosomal vehicles. After 48 h, DOX and HAuNS remained trapped in the endolysosomal vehicles (Fig. 5A). This observation contrasts with our earlier findings that DOX could be released from DOX@HAuNS at ~pH 5. It may be that in the microenvironment of endolysosomes, the detached DOX re-attached to HAuNS before the drug molecules had a chance to diffuse out of the vehicles. In contrast to DOX@HAuNS, free DOX was taken up by the tumor cells and distributed to cell nuclei 1 h after incubation (Fig. 5B). NIR laser irradiation (1.0 W/cm^2 for 3 min per treatment, 4 treatments over a 2-h period) caused release of DOX from DOX@HAuNS, and DOX was distributed to cell nuclei (Fig. 5B). Thus, it is possible to control intracellular DOX release from DOX@HAuNS and DOX@PEG-HAuNS by NIR laser irradiation.

Both DOX@HAuNS and DOX@PEG-HAuNS were cytotoxic against MDA-MB-231 cells in a dose-dependent manner. About 33.5% and 39.5% of cells were killed by DOX@HAuNS and DOX@PEG-HAuNS, respectively at an equivalent DOX concentration of 10 μg/mL (Fig. 6A). However, free DOX exhibited higher toxicity, with 77.4% cell killed at the same drug concentration. The lower cell killing potency with DOX@HAuNS and DOX@PEG-HAuNS could be attributed to relatively stable complexes formed between DOX and HAuNS and delayed DOX release inside cells. After NIR laser irradiation (2 W/cm^2 for 3 min per treatment, 4 treatments over a 2-h period), both DOX@HAuNS and DOX@PEG-HAuNS showed significant enhanced cell-killing effect toward cancer cells, with about 83.5% and 86.4% cell killed, respectively, at an equivalent DOX concentration of 10 μg/mL (Fig. 6A). HAuNS was not cytotoxic with Au concentrations ranging from 0.04 μg/mL to 160 μg/mL (Fig. 6B). This is consistent with literature findings that in general, Au-based nanoparticles are well tolerated.[14, 15] Plain unloaded HAuNS exhibited significant cell-killing effect (>69% cells killed), when cells incubated with HAuNS were treated with NIR laser at Au concentrations greater than 16 μg Au/mL (Fig. 6B). These results indicate that HAuNS produced significant photothermal ablation at concentrations greater than 16 μg Au/mL. At an Au concentration of 5.9 μg/mL (10 μg/mL equivalent DOX), 86.4% of cells were killed with combined DOX@PEG-HAuNS and NIR laser treatments. In comparison, treatments with combined HAuNS and NIR laser killed

only 40.6% of the cancer cells (Fig. 6B). The enhanced cytotoxicity of DOX@HAuNS and DOX@PEG-HAuNS at lower concentrations primarily resulted from DOX released upon NIR laser irradiation. Thus, at higher concentrations of DOX@HAuNS and DOX@PEG-HAuNS, both photothermal ablation and cytotoxic activity of DOX contributed to the killing of cancer cells.

Conclusion

In summary, this work presents HAuNS as a novel nanocarrier for drug delivery. This approach is advantageous in several aspects. First, HAuNS displayed exceptionally high drug loading capacity and stability as exemplified by DOX owing to the unique physicochemical characteristics of HAuNS. In particular, the hollow interior of the nanoparticles allowed significant increase in effective surface area for DOX attachment, resulting in 3.5-fold increase in DOX payload compared with solid AuNP of the same size, surface charge, and weight. Second, HAuNS mediated strong photothermal effect owing to their strong surface plasmon absorption in the NIR region. This property was exploited for controlled release of DOX from DOX@HAuNS using NIR light as the external stimulus to trigger drug release. Third, dual models of cell killing were integrated into a single nanodevice, i.e., photothermal ablation mediated by HAuNS and antitumor activity of DOX released from HAuNS upon NIR laser irradiation. This “two-punch” approach is expected to significantly increase the likelihood of cell killing and potentially overcome resistance to chemotherapeutic agents, making it a promising approach to cancer therapy.

Materials and Experiments

Reagents

DOX, methoxy-PEG-SH (MW, 5,000), PBS (pH 7.4), and the cell cytotoxicity kit for MTT assay were obtained from Sigma-Aldrich (St. Louis, MO). Trisodium citrate dehydrate (>99%), cobalt chloride hexahydrate (99.99%), sodium borohydride (99%), and chloroauric acid trihydrate (ACS reagent grade) were purchased from Fisher Scientific (Pittsburgh, PA) and were used as received. Methylene chloride (ACS grade) was obtained from Baxter Healthcare Corp (Deerfield, IL). Gold nanoparticles with average diameter of 41.5 nm were purchased from BB International (Madison, WI).

Cell Culture

MDA-MB-231 (human breast carcinoma) cells were maintained at 37°C in a humidified atmosphere containing 5% CO_2 in Dulbecco's modified Eagle's medium and 10% fetal bovine serum (Life Technologies, Inc., Grand island, NY).

Synthesis of HAuNS and Conjugation of PEG to HAuNS

HAuNS were synthesized according to a previously reported method.[30] Briefly, cobalt nanoparticles were first synthesized by deoxygenating deionized water containing 4.5 mL of 1 mol/L sodium borohydride, 2.8 mL of 0.1 mol/L sodium citrate, and 1.0 mL of 0.4 mol/L cobalt chloride. After chloroauric acid was added into the solution containing cobalt nanoparticles, the cobalt immediately reduced the gold ions onto the surface of cobalt nanoparticles, while at the same time it was oxidized to cobalt oxide. Any remaining cobalt core was further oxidized by air, resulting in the final product, HAuNS. The size of HAuNS was determined using dynamic light scattering on a Brookhaven 90 plus particle size analyzer (Holtsville, NY). UV-visible spectroscopy was recorded on a Beckman Coulter DU-800 UV-visible spectrometer (Fullerton, CA). The morphology of HAuNS was examined using a JEM 1010 transmission electron microscope (JEOL USA, Peabody, MA). The concentration of HAuNS was estimated by our previously reported method.[29] PEG-modified HAuNS (PEG-

HAuNS) were prepared according to our previous studies.[30] Briefly, HAuNS (5.0×10^{12} particles/mL) were added to argon-purged aqueous solution containing PEG-SH with various concentrations. The reaction was allowed to proceed overnight at room temperature. For purification, the reaction mixture was centrifuged at 14,000 rpm for 20 min, and the resulting pellet was resuspended with deionized water. The process was repeated twice to remove unreacted PEG molecules.

DOX Loading onto HAuNS and PEG-HAuNS

Aliquots of free DOX in water (1.0 mM, 0.02-0.3 mL) were added into an aqueous solution of HAuNS or PEG-HAuNS (1.0×10^{11} particles, 0.1 mL), and the mixtures were stirred at room temperature for 24 h. After centrifugation (14,000 rpm for 20 min), the precipitate was washed with PBS and centrifuged, and the washing cycle was repeated until the supernatant became colorless. All supernatants collected were pooled together, and the amount of free DOX in the supernatant was determined by spectrophotometry at 287 nm. DOX loading capacity (LC) was estimated using two methods. The first method indirectly measures attached DOX by determining the amount of unbound DOX in the supernatant according to Equation 1. The second method directly quantifies DOX attached to HAuNS after extraction of DOX from dried HAuNS with dimethyl sulfoxide according to Equation 2.

$$LC_{indirect} = (\text{Total DOX used} - \text{DOX in supernatant}) / (\text{Total Au used} + \text{Total DOX used} - \text{DOX in supernatant}) \times 100\% \quad \text{Equation 1}$$

$$LC_{direct} = \text{Total DOX extracted from HAuNS} / \text{Total particle weight} \times 100\% \quad \text{Equation 2}$$

DOX Release from HAuNS and PEG-HAuNS

The release studies were performed at room temperature. DOX@HAuNS or DOX@PEG-HAuNS ($\sim1.0\times10^{12}$ particles/mL) were dispersed in 2.0 mL PBS (10 mM, pH 7.4) in a 5-mL test tube. A laser probe (10-mm spot diameter) was placed on the side 5.0 cm from the center of the test tube. At predetermined time intervals, the samples were irradiated with NIR laser centered at 808 nm at an output power of 2.0 W/cm^2 for 3 min (Diomed 15 plus, Cambridge, UK). The nanoparticle solutions were centrifuged (14,000 rpm, 20 min) and supernatants withdrawn for analysis of DOX before and after NIR laser irradiation. The concentration of DOX in the supernatant was determined spectrophotometrically.

Cell Uptake of DOX@HAuNS and DOX@PEG-HAuNS

MDA-MB-231 cells were transferred and cultured onto 20-mm glass cover slips in a 24-well plate and allowed to grow for 2 days. Then the medium was replaced with 1 mL of fresh culture medium containing free DOX, DOX@HAuNS, or DOX@PEG-HAuNS. After incubation for 1 hr or 48 h, the cell monolayer on the cover slip was removed, repeatedly rinsed with PBS, and then mounted for microscopic examination. The cellular fluorescence and dark-field light scattering images were examined under a Zeiss Axio Observer.Z1 fluorescence microscope (Carl Zeiss MicroImaging GmbH, USA) equipped with a dark-field condenser.

In a separated experiment, MDA-MB-231 cells cultured on 20-mm glass cover slips were irradiated with NIR laser (1.0 W/cm^2 for 3 min per treatment, 4 treatments in 2 h). Cell nuclei were stained with DAPI. The cellular fluorescence and light scattering images were obtained as described in the preceding paragraph.

Cytotoxicity of DOX-HAuNS and DOX-PEG-HAuNS

A total of 2.0×10^4 cells were plated in 96-well plates and incubated for 24 h to allow the cells to attach. The cells were exposed to free DOX, DOX@HAuNS, or DOX@PEG-HAuNS with various DOX concentrations. The cells were or were not irradiated with NIR laser at an output power of 2 W/cm^2 (3 min per treatment, 4 treatments in 2 h). Then the cells were incubated at 37°C for a further 48 h. Cell survival efficiency was measured using the MTT assay according to the manufacturer suggested procedures. The data reported represented the means of triplicate measurements. In a separate experiment, the cells were exposed to HAuNS with various Au concentrations and then were or were not irradiated with NIR laser under the same conditions. Cell survival efficiency was measured after the incubation at 37°C for 48 h.

Acknowledgments

We thank Stephanie Deming for editing the article. This work was supported in part by the National Cancer Institute (grant R01 CA119387) and the John S. Dunn Foundation.

References

1. Davis SS. Coming of age of lipid-based drug delivery systems. Adv Drug Deliv Rev 2004;56(9):1241–2. [PubMed: 15109766]
2. Nishiyama N, Kataoka K. Current state, achievements, and future prospects of polymeric micelles as nanocarriers for drug and gene delivery. Pharmacol Ther 2006;112(3):630–48. [PubMed: 16815554]
3. Li C, Wallace S. Polymer-drug conjugates: recent development in clinical oncology. Adv Drug Deliv Rev 2008;60(8):886–98. [PubMed: 18374448]
4. Alexiou C, Arnold W, Klein RJ, Parak FG, Hulin P, Bergemann C, Erhardt W, Wagenpfeil S, Lubbe AS. Locoregional cancer treatment with magnetic drug targeting. Cancer Res 2000;60(23):6641–8. [PubMed: 11118047]
5. Jain TK, Morales MA, Sahoo SK, Leslie-Pelecky DL, Labhasetwar V. Iron oxide nanoparticles for sustained delivery of anticancer agents. Mol Pharm 2005;2(3):194–205. [PubMed: 15934780]
6. Murakami T, Ajima K, Miyawaki J, Yudasaka M, Iijima S, Shiba K. Drug-loaded carbon nanohorns: adsorption and release of dexamethasone *in vitro*. Mol Pharm 2004;1(6):399–405. [PubMed: 16028351]
7. Ajima K, Yudasaka M, Murakami T, Maigne A, Shiba K, Iijima S. Carbon nanohorns as anticancer drug carriers. Mol Pharm 2005;2(6):475–80. [PubMed: 16323954]
8. Liu Z, Chen K, Davis C, Sherlock S, Cao Q, Chen X, Dai H. Drug delivery with carbon nanotubes for *in vivo* cancer treatment. Cancer Res 2008;68(16):6652–60. [PubMed: 18701489]
9. Dhar S, Liu Z, Thomale J, Dai H, Lippard SJ. Targeted single-wall carbon nanotube-mediated Pt(IV) prodrug delivery using folate as a homing device. J Am Chem Soc 2008;130(34):11467–76. [PubMed: 18661990]
10. Feazell RP, Nakayama-Ratchford N, Dai H, Lippard SJ. Soluble single-walled carbon nanotubes as longboat delivery systems for platinum(IV) anticancer drug design. J Am Chem Soc 2007;129(27):8438–9. [PubMed: 17569542]
11. Liu Z, Sun X, Nakayama-Ratchford N, Dai H. Supramolecular chemistry on water-soluble carbon nanotubes for drug loading and delivery. ACS Nano 2007;1(1):50–6. [PubMed: 19203129]
12. Templeton AC, Wuelfing WP, Murray RW. Monolayer-protected cluster molecules. Acc Chem Res 2000;33(1):27–36. [PubMed: 10639073]
13. De M, Ghosh PS, Rotello VM. Applications of Nanoparticles in Biology. Adv Mater 2008;20(22):4225–4241.
14. Bhattacharya R, Mukherjee P. Biological properties of "naked" metal nanoparticles. Adv Drug Deliv Rev 2008;60(11):1289–306. [PubMed: 18501989]
15. Connor EE, Mwamuka J, Gole A, Murphy CJ, Wyatt MD. Gold nanoparticles are taken up by human cells but do not cause acute cytotoxicity. Small 2005;1(3):325–7. [PubMed: 17193451]

16. Cheng MM, Cuda G, Bunimovich YL, Gaspari M, Heath JR, Hill HD, Mirkin CA, Nijdam AJ, Terracciano R, Thundat T, Ferrari M. Nanotechnologies for biomolecular detection and medical diagnostics. Curr Opin Chem Biol 2006;10(1):11–9. [PubMed: 16418011]

17. Rosi NL, Mirkin CA. Nanostructures in biodiagnostics. Chem Rev 2005;105(4):1547–62. [PubMed: 15826019]

18. Baptista P, Pereira E, Eaton P, Doria G, Miranda A, Gomes I, Quaresma P, Franco R. Gold nanoparticles for the development of clinical diagnosis methods. Anal Bioanal Chem 2008;391(3): 943–50. [PubMed: 18157524]

19. Gibson JD, Khanal BP, Zubarev ER. Paclitaxel-functionalized gold nanoparticles. J Am Chem Soc 2007;129(37):11653–61. [PubMed: 17718495]

20. Cheng Y, S AC, Meyers JD, Panagopoulos I, Fei B, Burda C. Highly efficient drug delivery with gold nanoparticle vectors for *in vivo* photodynamic therapy of cancer. J Am Chem Soc 2008;130(32): 10643–7. [PubMed: 18642918]

21. Kim CK, Ghosh P, Pagliuca C, Zhu ZJ, Menichetti S, Rotello VM. Entrapment of hydrophobic drugs in nanoparticle monolayers with efficient release into cancer cells. J Am Chem Soc 2009;131(4): 1360–1. [PubMed: 19133720]

22. Chithrani BD, Chan WC. Elucidating the mechanism of cellular uptake and removal of protein-coated gold nanoparticles of different sizes and shapes. Nano Lett 2007;7(6):1542–50. [PubMed: 17465586]

23. Visaria RK, Griffin RJ, Williams BW, Ebbini ES, Paciotti GF, Song CW, Bischof JC. Enhancement of tumor thermal therapy using gold nanoparticle-assisted tumor necrosis factor-alpha delivery. Mol Cancer Ther 2006;5(4):1014–20. [PubMed: 16648573]

24. Ghosh PS, Kim CK, Han G, Forbes NS, Rotello VM. Efficient gene delivery vectors by tuning the surface charge density of amino acid-functionalized gold nanoparticles. ACS Nano 2008;2(11): 2213–8. [PubMed: 19206385]

25. Lee JS, Green JJ, Love KT, Sunshine J, Langer R, Anderson DG. Gold, poly(beta-amino ester) nanoparticles for small interfering RNA delivery. Nano Lett 2009;9(6):2402–6. [PubMed: 19422265]

26. Elbakry A, Zaky A, Liebl R, Rachel R, Goepferich A, Breunig M. Layer-by-layer assembled gold nanoparticles for siRNA delivery. Nano Lett 2009;9(5):2059–64. [PubMed: 19331425]

27. Dhar S, Reddy EM, Shiras A, Pokharkar V, Prasad BL. Natural gum reduced/stabilized gold nanoparticles for drug delivery formulations. Chemistry 2008;14(33):10244–50. [PubMed: 18850613]

28. Kumar SA, Peter YA, Nadeau JL. Facile biosynthesis, separation and conjugation of gold nanoparticles to doxorubicin. Nanotechnology 2008;19(49)

29. Melancon MP, Lu W, Yang Z, Zhang R, Cheng Z, Elliot AM, Stafford J, Olson T, Zhang JZ, Li C. *In vitro* and *in vivo* targeting of hollow gold nanoshells directed at epidermal growth factor receptor for photothermal ablation therapy. Mol Cancer Ther 2008;7(6):1730–1739. [PubMed: 18566244]

30. Lu W, Xiong C, Zhang G, Huang Q, Zhang R, Zhang JZ, Li C. Targeted photothermal ablation of murine melanomas with melanocyte-stimulating hormone analog-conjugated hollow gold nanospheres. Clin Cancer Res 2009;15(3):876–86. [PubMed: 19188158]

31. Schwartzberg AM, Olson TY, Talley CE, Zhang JZ. Synthesis, characterization, and tunable optical properties of hollow gold nanospheres. J Phys Chem B 2006;110(40):19935–19944. [PubMed: 17020380]

32. Fan C, Wang S, Hong JW, Bazan GC, Plaxco KW, Heeger AJ. Beyond superquenching: hyper-efficient energy transfer from conjugated polymers to gold nanoparticles. Proc Natl Acad Sci U S A 2003;100(11):6297–301. [PubMed: 12750470]

33. Peer D, Karp JM, Hong S, Farokhzad OC, Margalit R, Langer R. Nanocarriers as an emerging platform for cancer therapy. Nat Nanotechnol 2007;2(12):751–60. [PubMed: 18654426]

34. Maxfield FR, McGraw TE. Endocytic recycling. Nat Rev Mol Cell Biol 2004;5(2):121–32. [PubMed: 15040445]

35. Ji XJ, Shao RP, Elliott AM, Stafford RJ, Esparza-Coss E, Bankson JA, Liang G, Luo ZP, Park K, Markert JT, Li C. Bifunctional gold nanoshells with a superparamagnetic iron oxide-silica core suitable for both MR imaging and photothermal therapy. J Phys Chem C 2007;111(17):6245–6251.

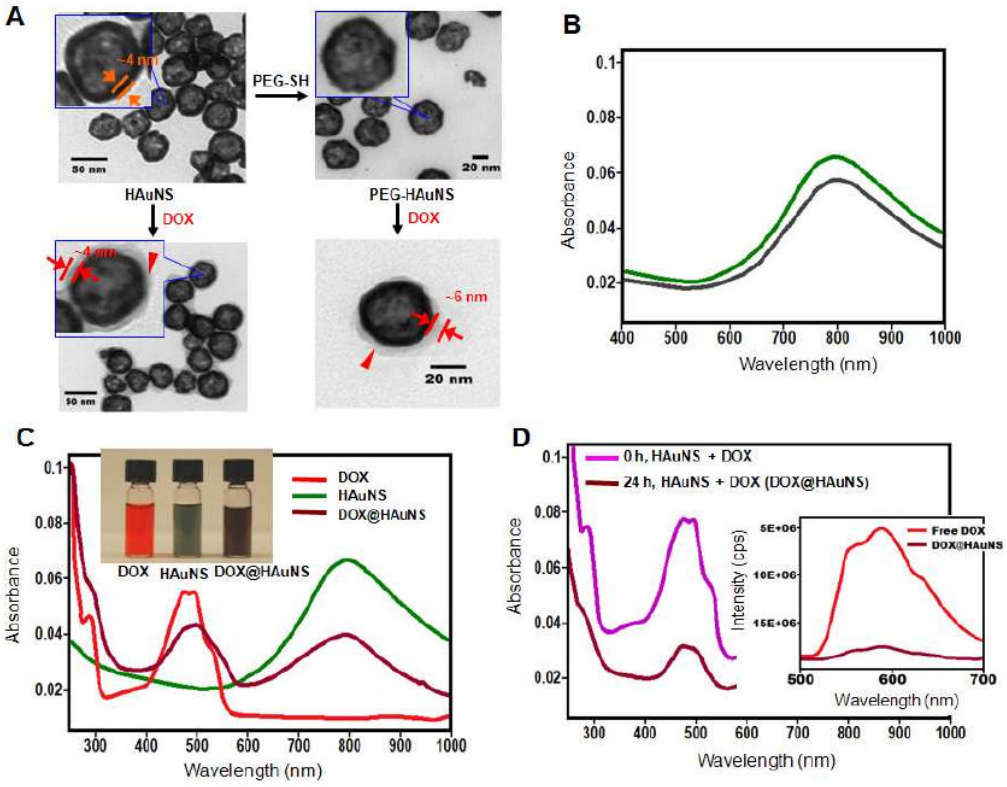

Fig. 1.

Fabrication and characterization of DOX-loaded hollow gold nanospheres (DOX@HAuNS). **A**, Schematic of HAuNS synthesis and TEM images of plain and DOX-loaded HAuNS (DOX@HAuNS and DOX@PEG-HAuNS). **B**, Absorption spectra of HAuNS and PEG-HAuNS. **C**, Absorbance spectra of free DOX (red), HAuNS (green), and DOX@HAuNS (brown). Inset: Photograph of aqueous solutions of free DOX, HAuNS, and DOX@HAuNS. DOX@HAuNS displayed absorption peaks characteristic of both DOX and HAuNS. **D**, Absorbance spectra of initial physical mixture of DOX and HAuNS (purple) and the complexes of DOX and HAuNS after 24h of incubation (brown). Inset: Fluorescence spectra of solutions of free DOX (red) and DOX@HAuNS (brown; excitation at 488 nm) with the same DOX concentration. Significant fluorescence quenching was observed for DOX@HAuNS.

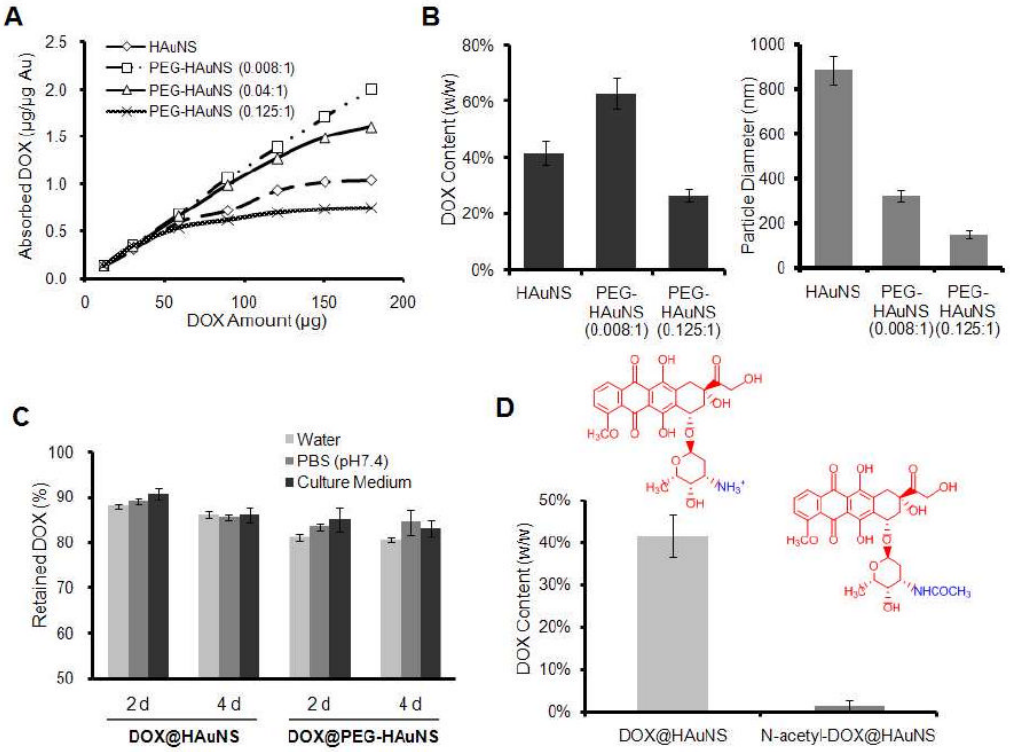

Fig. 2.

A, Langmuir adsorption isotherms showing the adsorption of DOX by HAuNS and PEG-HAuNS with various PEG:Au molar ratios. The absorbed DOX was plotted against the initial amount of DOX in the solution. **B**, Comparison of DOX payload (left) and particle size (right) between DOX@HAuNS and DOX@PEG-HAuNS at the maximal DOX loading. Low PEG density increased DOX payload. PEGylation stabilized DOX-loaded HAuNS. Particle size was measured by dynamic light scattering after a mild water-bath ultrasound treatment. **C**, Stability of DOX@HAuNS and DOX@PEG-HAuNS in various media. **D**, Blocking the free NH_2 group in DOX substantially reduced DOX loading to HAuNS.

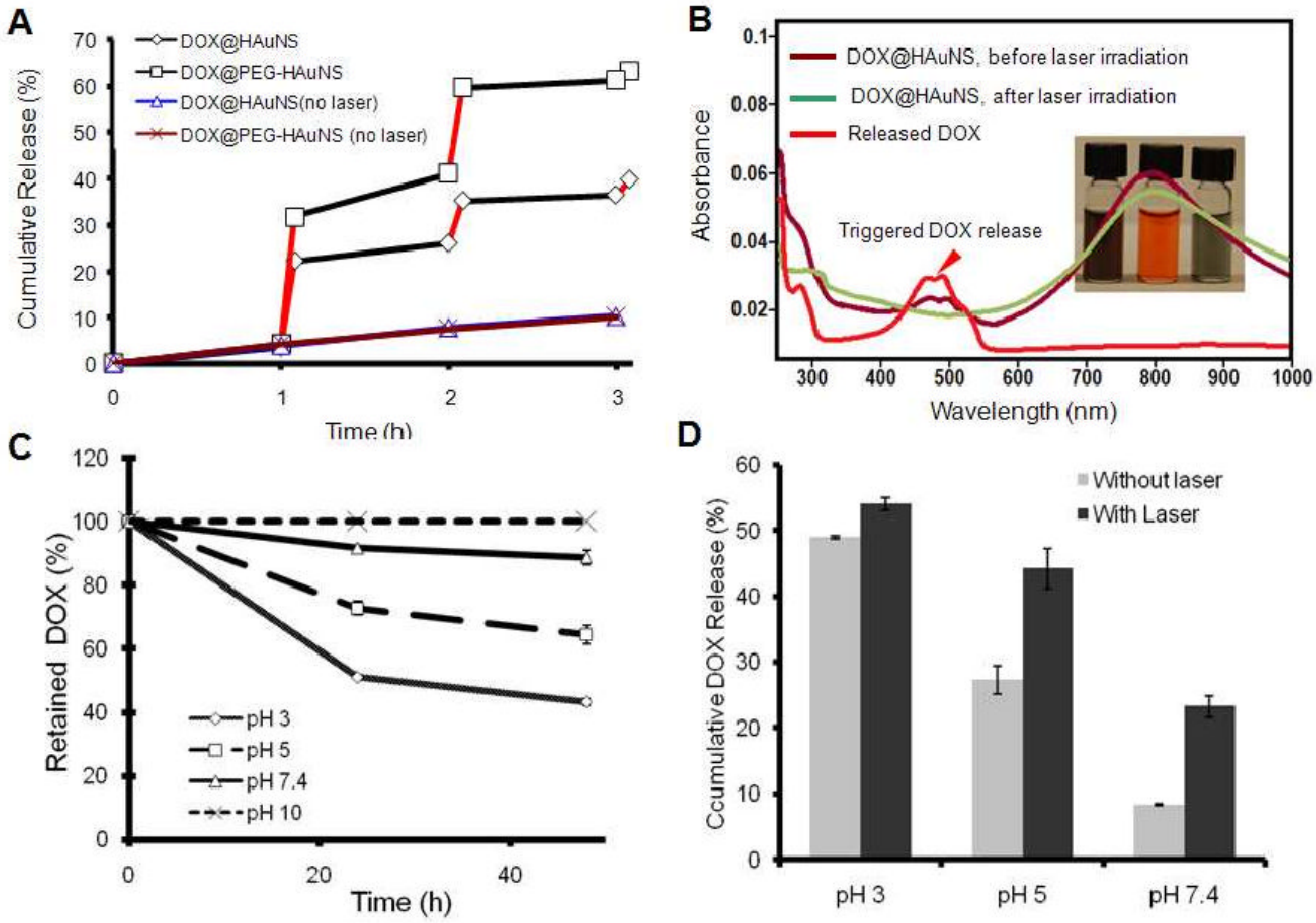

Fig. 3.

NIR light triggered release of DOX from DOX@HAuNS and DOX@PEG-HAuNS. **A**, DOX release profiles in the presence and absence of NIR laser. Irradiation with NIR laser caused rapid DOX release during NIR exposure (5 min, red lines), and the release was turned off when laser was switched off. **B**, Absorption spectra of DOX@HAuNS before and after NIR laser irradiation. Inset: Photograph of aqueous solutions of (a) DOX@HAuNS before laser irradiation, (b) released DOX collected in the supernatant, and (c) DOX@HAuNS after complete release of DOX. **C**, Effect of pH on DOX retention on PEG-HAuNS. **D**, Comparison of NIR light-triggered

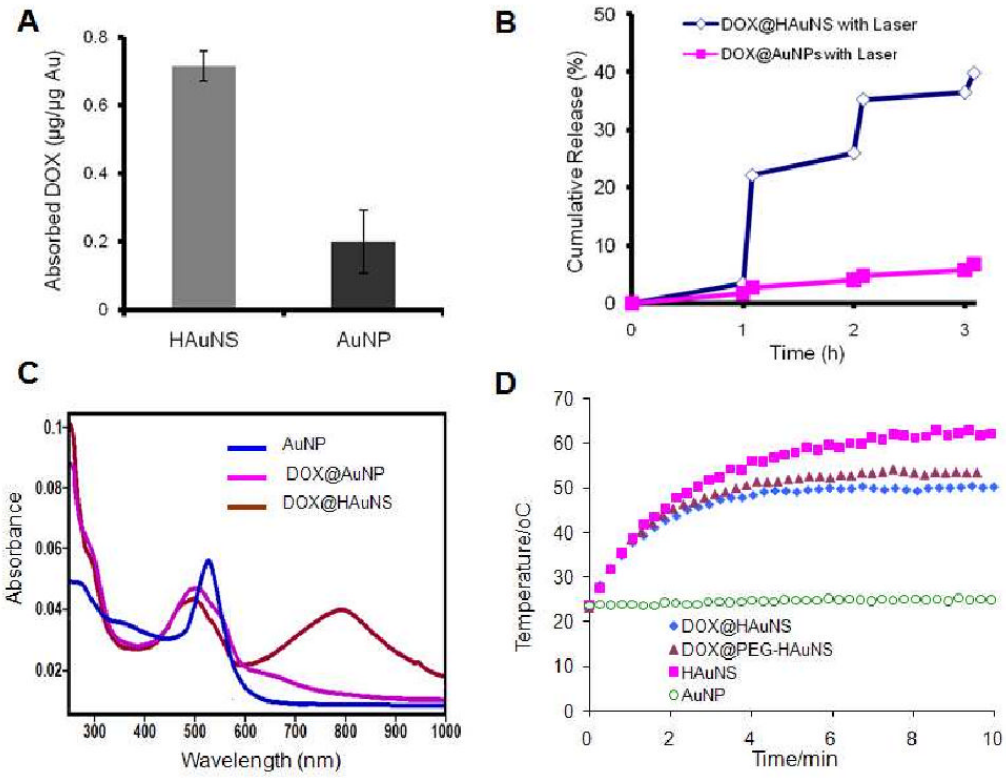

Fig. 4.

Comparison between hollow gold nanospheres (HAuNS) and solid gold nanoparticles (AuNP). **A**, Comparison of DOX payload between HAuNS and solid AuNP. **B**, Release of DOX from DOX@HAuNS (blue line) and DOX@AuNP (pink line) under repeated NIR laser exposure. **C**, Comparison of absorption spectra among AuNP, DOX@AuNP, and DOX@HAuNS. **D**, Temperature change measured over a period of 10 min of exposure to NIR light at an output power of 5.0 W/cm^2. All nanoparticles had the same concentration of 0.7×10^{11} particles/mL. Temperatures were measured according to a previously reported method.[35]

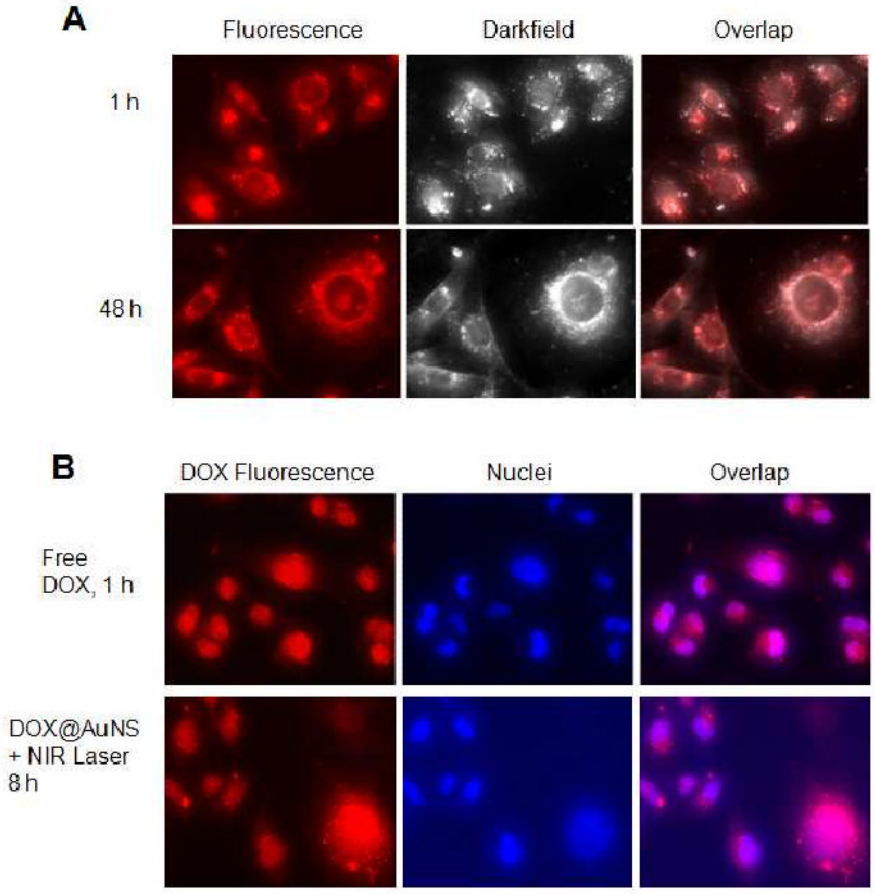

Fig. 5.

Uptake of DOX@HAuNS and free DOX in MDA-MB-231 breast cancer cells. **A**, Cell uptake of DOX@HAuNS after 1 h and 48 h of incubation. The reflectance of HAuNS was visualized using a dark-field condenser. The red color from the fluorescence signal of DOX@HAuNS was localized in spots in the cytoplasm. **B**, Cell uptake of free DOX and DOX@HAuNS treated with NIR laser (1.0 W/cm^2 for 3 min per treatment, 4 treatments over 2 h, incubated for 8 h). Cell nuclei were counterstained with DAPI (blue). The red fluorescence signal from DOX in DOX@HAuNS was localized to the cell nuclei after NIR laser irradiation, indicating intracellular release of DOX from DOX@HAuNS upon NIR exposure.

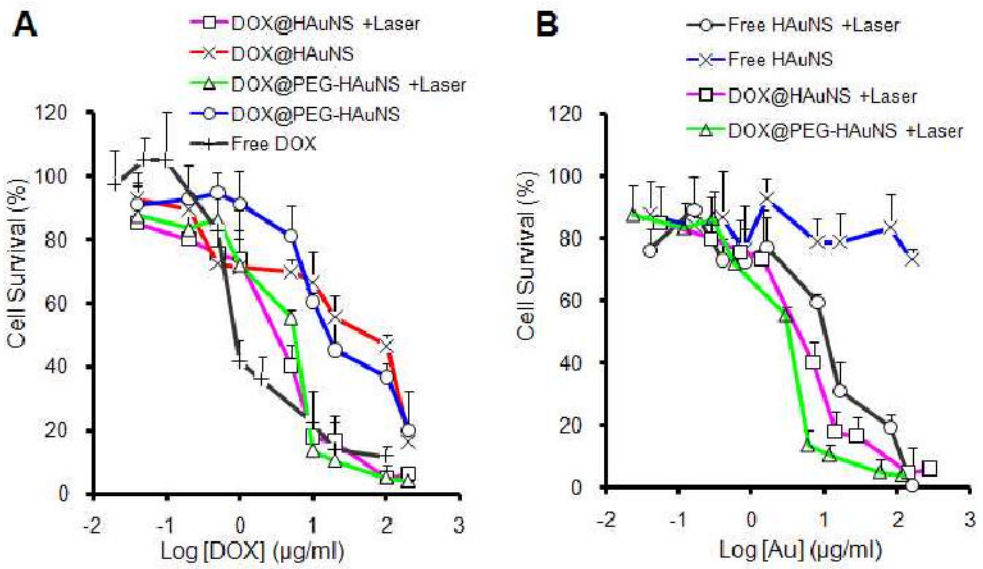

Fig. 6.

Cell survival as a function of DOX concentration (left) and Au concentration (right). MDA-MB-231 cells were either not exposed to NIR light or irradiated with NIR light (2 W/cm^2 for 3 min per treatment, 4 treatments over 2 h). The viability of cells was determined using the MTT assay. Data represent mean ± standard deviation of triplicate experiments.